MITSUBISHI ELECTRIC RESEARCH LABORATORIES
http://www.merl.com

# From Reeds-Shepp's paths to continuous curvature path- Part I: transition schemes &algorithms

Dai, J.; Wang, Y.; Bortoff, S.A.; Burns, D.J.

TR2017-122 August 2017

## Abstract

This work considers real-time continuous curvature (CC) path planning for car-like robots. It is motivated by the fact that Reeds-Shepp's (RS) based path planning remains unmatched in terms of computation efficiency and reliability when compared with various CC path planning results. Similar to [1], this paper post-processes RS paths to enforce the CC property, while ensuring CC paths contained in a neighborhood of the RS paths to maintain obstacle clearance. Targeting to alleviate concerns about reliability and computational efficiency, we exploit the geometric insights casted by  tangency conditions [2] to post-process RS paths. Specifically, distinctive postprocessing scheme is devised offline for each type of discontinuous curvature junctions. The proposed schemes, though suboptimal, are straightforward, and result in CC path planning with guaranteed completeness at the negligible increase of computation. Effectiveness of proposed schemes and resultant algorithms is validated by numerical simulations.

*IEEE Conference on Control Technology and Applications*

This work may not be copied or reproduced in whole or in part for any commercial purpose. Permission to copy in whole or in part without payment of fee is granted for nonprofit educational and research purposes provided that all such whole or partial copies include the following: a notice that such copying is by permission of Mitsubishi Electric Research Laboratories, Inc.; an acknowledgment of the authors and individual contributions to the work; and all applicable portions of the copyright notice. Copying, reproduction, or republishing for any other purpose shall require a license with payment of fee to Mitsubishi Electric Research Laboratories, Inc. All rights reserved.

Copyright © Mitsubishi Electric Research Laboratories, Inc., 2017
201 Broadway, Cambridge, Massachusetts 02139

# From Reeds-Shepp's paths to continuous curvature paths–Part I: transition schemes & algorithms

Jin Dai, Yebin Wang, Scott A. Bortoff, and Daniel J. Burns

*Abstract*— **This work considers real-time continuous curvature (CC) path planning for car-like robots. It is motivated by the fact that Reeds-Shepp's (RS) based path planning remains unmatched in terms of computation efficiency and reliability when compared with various CC path planning results. Similar to [1], this paper post-processes RS paths to enforce the CC property, while ensuring CC paths contained in a neighborhood of the RS paths to maintain obstacle clearance. Targeting to alleviate concerns about reliability and computational efficiency, we exploit the geometric insights casted by $\mu-$tangency conditions [2] to post-process RS paths. Specifically, distinctive post-processing scheme is devised offline for each type of discontinuous curvature junctions. The proposed schemes, though sub-optimal, are straightforward, and result in CC path planning with guaranteed completeness at the negligible increase of computation. Effectiveness of proposed schemes and resultant algorithms is validated by numerical simulations.**

## I. Introduction

Path planning for robots has been extensively investigated over decades, with the consideration of kinematic, dynamic and environmental constraints [3]–[5]. A vast majority of research efforts have been oriented to robots with nonholonomic dynamics [6]–[9] and particularly car-like robots, due to their widespread applications [10].

Pioneering work [7], [8] has shown that shortest length paths, known as Reeds-Shepp (RS) paths, are composition of line segments and tangential circular arcs of the minimum turning radius. Nevertheless, RS paths possess a finite number of discontinuous curvature junctions (DCJs), which results in stationary steering, a cause of extra tire wearing.

Aiming to address limitations of RS paths, many contributions proposed continuous curvature (CC) paths for car-like robots. Work [11]–[13] established the existence of shortest length CC paths, which consist of clothoid curves and line segments; however, they exhibit infinite chattering at the presence of line segments. This discovery motivates search for sub-optimal CC paths. For instance, work [2], [13] proposed a group of sub-optimal CC paths, which are formed of clothoid turns and lines. The sub-optimal CC paths are generalization of RS paths because they share exactly the same patterns. An extension to [2], [13] can be found in [14], which offers analytical formula to compute such CC paths. Work [15] planed CC paths based on Bézier curve fitting, and [16] developed a numerically efficient planning scheme, which is only applicable to forward-moving robots.

The aforementioned prior art, assuming obstacle-free environment, are typically employed to realize local steering in decomposition-based path planning [4], [9], [17]. It is understood that exploration of collision-free configuration space involves a huge amount of steering operations. In order to achieve real-time path planning, the computational efficiency of the underlying steering algorithms is of paramount importance. Recent work [14] benchmarks the RS steering and a sub-optimal CC steering and demonstrates that the latter is about 10 times slower.

This work performs CC path planning, with the hope to achieve similar computational efficiency as the RS path planning. The proposed CC path planning contains two stages: first an RS path is computed, where the RS path is collision-free with a tolerance; then a CC path is constructed according to the RS path. The resultant CC path has to stay inside a neighborhood of the RS path, indicated by the tolerance, to ensure collision-free. It is noteworthy that similar idea has been exploited in [1]. However, work [1] resorts to optimal control theory and ends up with solving boundary value problems. Instead, by utilizing $\mu-$tangency conditions [2], this work proposes transition schemes to treat DCJs and develops algorithms, which guarantee successful construction of the CC path in an efficient way.

The remainder of this paper is organized as follows. Section II introduces kinematic models of a car-like robot and formulates the RS path post-processing problem. In Section III, we present CC transition schemes and algorithms to accomplish such transitions. Section IV validates the proposed schemes and algorithms by simulation. Concluding remarks are made in Section V.

## II. Preliminaries

A car-like robot, illustrated in Fig. 1, is equipped with a front-fixed steering wheel and fixed parallel rear wheels. The point $R$ is located in the mid of the rear wheels. The robot pose is uniquely described by a triple $(x, y, \theta)$ where $(x, y)$ represent the coordinates of $R$ in the global frame and $\theta$ is the orientation angle of the robot with respect to the $x$-axis. The robot has a wheelbase $b$, and a steering angle $\phi$.

J. Dai is the Department of Electrical Engineering, University of Notre Dame, Notre Dame, IN 46556, USA (e-mail: jdai1@nd.edu). This work was done during J. Dai's internship at Mitsubishi Electric Research Laboratories.

Y. Wang, S. A. Bortoff, and D. J. Burns are with Mitsubishi Electric Research Laboratories, 201 Broadway, Cambridge, MA 02139, USA. email: {yebinwang@ieee.org, bortoff@merl.com, burns@merl.com}

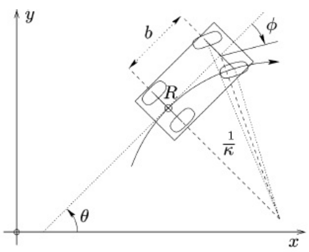

Fig. 1: A car-like robot

### A. RS Paths

Assume that the robot shown in Fig. 1 moves within a planar environment $\mathcal{W} \subseteq \mathbb{R}^2$. A *path* $\mathcal{P}$ is a mapping from $\mathbb{R}$ to the *configuration space* $\mathcal{C} = \mathcal{W} \times \mathbb{S}^1$, giving a configuration $q(s) = (x(s), y(s), \theta(s))$ for each $s \in [0, l]$, where $l$ is the total length of $\mathcal{P}$. Intuitively, $\mathcal{P}$ is a continuous curve in $\mathcal{C}$. Given an initial configuration $q_0$ and a finial configuration $q_f$, a path $\mathcal{P}$ is said to be *feasible* if $\mathcal{P}(0) = q_0$ and $\mathcal{P}(l) = q_f$ and it can be followed by the car-like robot. Work [8] established shortest path solutions, termed as RS paths, based on the following model

$$\begin{pmatrix} \dot{x} \\ \dot{y} \\ \dot{\theta} \end{pmatrix} = \begin{pmatrix} \cos\theta \\ \sin\theta \\ 0 \end{pmatrix} v + \begin{pmatrix} 0 \\ 0 \\ 1 \end{pmatrix} u, \tag{1}$$

where $v$ is the driving velocity of the rear wheels and $u$ the rate of orientation. Note that $v \in [-1, 1]$, and $u \in [-1, 1]$. RS paths can be categorized into 12 classes, and admit a total of 48 patterns [8]. All classes and patterns are listed in Table I, where $C$ stands for a circular arc and $S$ stands for a line segment; while $L$ and $R$ specify left and right turns with $+$ or $-$ denoting forward or backward motion, respectively. The subscripts denote the (absolute) angular value of a certain circular arc and $|$ represents a cusp.

TABLE I: Classes of RS paths

| Classes | Patterns |
|---|---|
| $CSC - 1$ | L+S+L+, L-S-L-, R+S+R+, R-S-R- |
| $CSC - 2$ | L+S+R+, L-S-R-, R+S+L+, R-S-L- |
| $C\vert C\vert C$ | L+R-L+, L-R+L-, R+L-R+, R-L+R- |
| $C\vert CC$ | L+R-L-, L-R+L+, R+L-R-, R-L+R+ |
| $CC\vert C$ | L+R+L-, L-R-L+, R+L+R-, R-L-R+ |
| $CC_u\vert C_uC$ | L+R+L-R-, L-R-L+R+, R+L+R-L-, R-L-R+L+ |
| $C\vert C_uC_u\vert C$ | L+R-L-R+, L-R+L+R-, R+L-R-L+, R-L+R+L- |
| $C\vert C_{\frac{\pi}{2}}SC - 1$ | L+R-S-R-, L-R+S+R+, R+L-S-L-, R-L+S+L+ |
| $C\vert C_{\frac{\pi}{2}}SC - 2$ | L+R-S-L-, L-R+S+L+, R+L-S-R-, R-L+S+R+ |
| $CSC_{\frac{\pi}{2}}\vert C - 1$ | L+S+L+R-, L-S-L-R+, R+S+R+L-, R-S-R-L+ |
| $CSC_{\frac{\pi}{2}}\vert C - 2$ | L+S+R+L-, L-S-R-L+, R+S+L+R-, R-S-L-R+ |
| $C\vert C_{\frac{\pi}{2}}SC_{\frac{\pi}{2}}\vert C$ | L+R-S-L-R+, L-R+S+L+R-,<br>R+L-S-R-L+, R-L+S+R+L- |

### B. CC Path Planning

A major downside of RS paths is the presence of DCJs. This work addresses DCJs in RS paths by constructing a solution of the following model

$$\begin{pmatrix} \dot{x} \\ \dot{y} \\ \dot{\theta} \\ \dot{\kappa} \end{pmatrix} = \begin{pmatrix} \cos\theta \\ \sin\theta \\ \kappa \\ 0 \end{pmatrix} v + \begin{pmatrix} 0 \\ 0 \\ 0 \\ 1 \end{pmatrix} \bar{\sigma}, \tag{2}$$

where the curvature $\kappa$ is an extra configuration parameter. System (2) has two control inputs: $v$ and the steering rate $\bar{\sigma}$. The relationship between $\phi$, $\kappa$ and $\bar{\sigma}$ is as follows:

$$\kappa = \frac{\tan\phi}{b}, \ \bar{\sigma} = \dot{\kappa} = \frac{\dot{\phi}}{b\cos^2\phi}.$$

With mechanical constraint on the steering wheel, $|\phi| \leq \phi_{\max}$, system (2) is subject to constraints

$$|v| \leq v_{\max}, \ |\kappa| \leq \kappa_{\max}, \ |\bar{\sigma}| \leq \bar{\sigma}_{\max}, \tag{3}$$

where $\kappa_{\max} = \tan\phi_{\max}/b$ and $\bar{\sigma}_{\max} = |\dot{\phi}|_{\max}/b$. Thus, the set of admissible control inputs is defined by

$$\mathcal{U} = \{u \in \mathfrak{U} : u(t) \in U, t \in [0, T_f]\},$$

where $\mathfrak{U}$ is the set of all measurable functions defined over $[0, T_f]$, and $U := [-v_{\max}, v_{\max}] \times [-\bar{\sigma}_{\max}, \bar{\sigma}_{\max}]$. For a vector $\zeta \in \mathbb{R}^n$, $\|\zeta\|$ denotes the standard 2-norm. Denote $\epsilon$ a small positive constant. The continuous curvature path planning problem aims to design a feasible and sub-optimal path in the augmented configuration space $\mathcal{C}' := \mathcal{C} \times [-\kappa_{\max}, \kappa_{\max}]$.

*Problem 1:* Given an RS path $\mathcal{P}_{RS}$ connecting initial/final configurations $q_0$ and $q_f$ in $\mathcal{C}'$, find a continuous curvature path $\mathcal{P}_{CC}$ with a finite $l$ such that

(i) $\mathcal{P}_{CC}(0) = q_0, \mathcal{P}_{CC}(l) = q_f$;
(ii) $\mathcal{P}_{CC}$ satisfies (2)-(3) for certain $[v, \bar{\sigma}] \in \mathcal{U}$;
(iii) $\mathcal{P}_{CC}$ remains in a neighborhood $B(\mathcal{P}_{RS}, \epsilon)$.

Problem 1 leverages the design freedom $v$ and $\epsilon$ to post-process RS paths into CC paths. It is well-posed, i.e., its solutions are guaranteed to exist. This claim can be loosely shown by the following argument. By treating the path length $s$ as the independent variable, system (2) can be rewritten $dx/ds = \cos\theta, dy/ds = \sin\theta, d\theta/ds = \kappa, d\kappa/ds = \bar{\sigma}/v$. Let us define a velocity profile $v_{cc}$ along $P_{rs}$, where $v_{cc}$ takes a small value $\bar{v}$ in neighborhoods of DCJs. This means that around DCJs, $d\kappa/ds$ is large, and thus instantaneous curvature changes of $P_{rs}$ can be approximated well. Each $v_{cc}$ gives rise to a CC path $P_{cc}$,by integrating system (2). By choosing different $\bar{v}$, one can obtain a family of CC paths $P_{cc}(\bar{v})$, which are parameterized by $\bar{v}$ and have continuous dependence on it. As $\bar{v} \to 0$, $P_{cc}(\bar{v}) \to P_{rs}$. Hence, given a neighborhood $B(P_{rs}, \epsilon)$, one can always find $\hat{v} > 0$ such that as long as $0 < \bar{v} < \hat{v}$ around DCJs, the CC path $P_{cc}(\bar{v})$ satisfies conditions in Problem 1.

### C. Clothiod Turns

CC path planning can be fulfilled by combining clothoid turns (CTs) and line segments in the similar manner as the RS path [2]. This section overviews clothoid, CT, and CC circle. Details can be found in [2].

A clothoid is a curve whose curvature $\kappa$ varies linearly with respect to its arc length $s$, i.e., $\kappa(s) = \sigma s + s_0$, where $\sigma$ is the sharpness of the clothoid and $s_0$ is the initial arc length. Take $s_0 = 0$ for simplicity. Integrating system (2) gives the configuration along the clothoid

$$q(s) = \begin{pmatrix} x(s) \\ y(s) \\ \theta(s) \\ \kappa(s) \end{pmatrix} = \begin{pmatrix} \sqrt{\pi/\sigma_{\max}} C_f\left(\dfrac{s}{\sqrt{\pi/\sigma_{\max}}}\right) \\ \sqrt{\pi/\sigma_{\max}} S_f\left(\dfrac{s}{\sqrt{\pi/\sigma_{\max}}}\right) \\ \frac{1}{2}\sigma_{\max} s^2 \\ \sigma_{\max} s \end{pmatrix},$$

where $C_f(s) = \int_0^s \cos\frac{\pi}{2}\tau^2 d\tau$ and $S_f(s) = \int_0^s \sin\frac{\pi}{2}\tau^2 d\tau$ are the Fresnel cosine and sine integrals, respectively. For a clothoid beginning with $q_s$ and ending at $q_f$, it has a deflection $\delta = \theta_f - \theta_s$. Given $\kappa_{\max}$ and $\sigma_{\max}$, the clothoid has a constant deflection $\delta_c = \kappa_{\max}^2/(2\sigma_{\max})$ and a constant arc length $s = \kappa_{\max}/\sigma_{\max}$.

The deflection of a CT can be defined exactly the same as a clothoid. Depending on its deflection $\delta$, a CT could consist of up to two clothoids and one circular arc. Fig. 2 illustrates a CT performing a left forward turn maneuver, where without loss of generality, the CT begins with $q_s = (0, 0, 0, 0)$. The CT, exemplifying case $2\delta_c \leq \delta < 2\delta_c + \pi$, consists of

(i) a clothoid from $q_s$ to $q_1$, with sharpness $\sigma_{\max}$;
(ii) a circular arc of radius $\kappa_{\max}^{-1}$ and of angle $\delta - 2\delta_c$, starting from $q_1$ and ending at $q_2$;
(iii) a second clothoid starting from $q_2$ with sharpness $-\sigma_{\max}$ and ending at $q_f$.

When $\delta = 0$, the CT reduces to a line segment of length $2R_\Omega \sin\mu$. For $0 \leq \delta < 2\delta_c$, a clothoid of sharpness $\sigma \leq \sigma_{\max}$ and a symmetric clothoid of sharpness $-\sigma$ are used in the CT, where the desired sharpness $\sigma$ is given by

$$\sigma = \frac{\pi\left(\cos\frac{\delta}{2} C_f\left(\sqrt{\frac{\delta}{\pi}}\right) + \sin\frac{\delta}{2} S_f\left(\sqrt{\frac{\delta}{\pi}}\right)\right)^2}{R_\Omega^2 \sin^2\left(\frac{\delta}{2} + \mu\right)},$$

and the length of each clothoid is $\sqrt{\delta/\sigma}$. The case with $2\delta_c + \pi \leq \delta < 2\pi$ corresponds to left backward motions, and can be treated similarly.

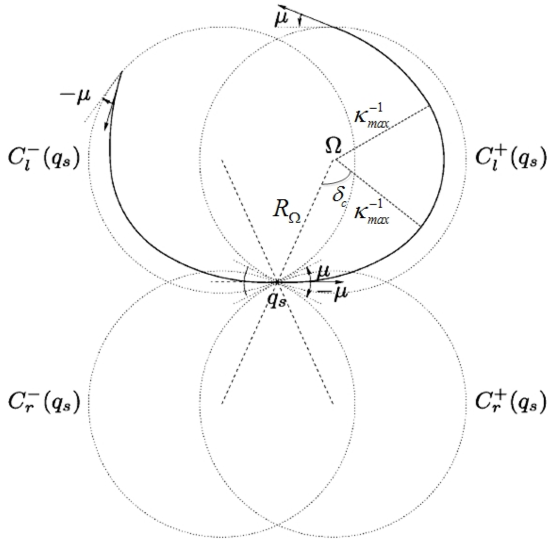

Fig. 2: CC circles $C_l^+$, $C_r^+$, $C_l^-$ and $C_r^-$ originated at $q_s$

A crucial concept in simplifying CC path planning from geometric perspective is CC Circle. Fig. 2 shows four CC circles associated with a configuration $q_s$, where $C_l^+(q_s), C_l^-(q_s), C_r^+(q_s), C_r^-(q_s)$ correspond to a left forward CT, a left backward CT, a right forward CT, and a right backward CT, respectively. Interestingly, each CC circle has exactly the same center as the circular arc of its respective CT. For instance, $\Omega$, the center of CC circle $C_l^+(q_s)$, coincides with the center of the circular arc which is tangential to the robot orientation at $q_1$. Coordinates of $\Omega$ are given by

$$\begin{pmatrix} x_\Omega \\ y_\Omega \end{pmatrix} = \begin{pmatrix} x_1 - \kappa_{\max}^{-1}\sin\theta_1 \\ y_1 + \kappa_{\max}^{-1}\cos\theta_1 \end{pmatrix}. \tag{4}$$

Given $\kappa_{\max}$ and $\sigma_{\max}$, the CC circle radius is given by

$$\begin{pmatrix} R_\Omega \\ \mu \end{pmatrix} = \begin{pmatrix} \sqrt{x_\Omega^2 + y_\Omega^2} \\ \arctan\dfrac{x_\Omega}{y_\Omega} \end{pmatrix}, \tag{5}$$

where $\mu$ is the angle between the robot orientation and the tangent vector of the CC circle at $q_s$.

## III. Continuous Curvature Transitions

Classes of RS paths in Table I reveal that DCJs occur at connections between straight line segments and circular arcs, specifically, $SC, CS, CC, C|C$. This section develops schemes to treat these four types of DCJs. That is, we work on Problem 1 with $P_{rs}$ being restricted to a simple RS path including only one DCJ.

### A. SC Transition

We investigate how to make a CC transition between a line and a circular arc. Without loss of generality, this corresponds to solve the following problem.

*Problem 2:* Let a simple RS path $\mathcal{P}_{RS}^{SC}$ consist of

(i) *A line S* described by $-\infty < x_0 \leq x \leq 0$ and $y = 0$;

(ii) *A circular arc* $C$, which is tangent to $S$ at the origin $(0, 0)$. The radius and angle of $C$ are given by $\kappa_{\max}^{-1}$ and $\theta$, respectively.

Construct a CC path $\mathcal{P}_{CC}$ which remains in $B(\mathcal{P}_{RS}^{SC}, \epsilon)$ while satisfying conditions (i)-(ii) in Problem 1.

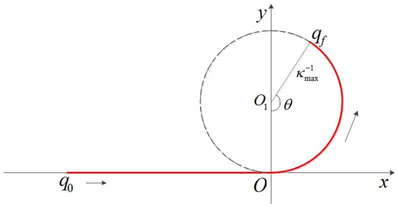

Fig. 3: A simple RS path: $SC$ type

The simple RS path $\mathcal{P}_{RS}^{SC}$ is depicted in Fig. 3.

*1) SC Transition Scheme:* Due to space limitation, we assume $\theta > 2\delta_c$. The following $SC$ transition scheme is proposed to make CC connection between $S$ and $C$

(i) A forward straight line segment that starts from the initial configuration $q_0 = (x_0, 0, 0, 0)$ and ends at the configuration $q_s = (x^*, 0, 0, 0)$ with $x_0 \leq x^* \leq 0$.
(ii) A forward right CT that starts from the configuration $q_s = (x^*, 0, 0, 0)$ and ends at $q_1 = (x_1, y_1, \delta, 0)$ with a deflection $\delta < 0$;
(iii) A forward left CT with a deflection $-\delta$ that starts from $q_1$ and ends at a configuration $q_2 = (x_2, y_2, 0, 0)$.
(iv) A forward left clothoid that connects $q_2$ and $q_3 = (x_3, y_3, \delta_c, \kappa_{\max})$, such that the point $(x_3, y_3) \in C$.

*Remark 1:* In the case that $\delta < 2\delta_c$, one can find $\sigma_{SC} \geq \sigma_{\max}$ such that the forward left clothoid with $\sigma_{SC}$ yields a deflection $\delta_{SC} \leq \delta/2$. A continuous curvature connection can be formed between the forward left clothoid and the circular arc in $\mathcal{P}_{RS}^{SC}$ .

Fig. 4 illustrates a procedure to determine parameters in the $SC$ transition scheme, i.e., $q_s, q_1, q_2$.

(i) As depicted by Fig. 4, both the CC Circle $C_l^+(q_2)$ and the circular arc $C$ share the same center $\Omega_3 = (0, \kappa_{\max}^{-1})$. Coordinates of $q_2$ are then computed by

$$q_2 = \begin{pmatrix} x_2 \\ y_2 \\ \theta_2 \\ \kappa_2 \end{pmatrix} = \begin{pmatrix} R_\Omega \cos\left(-\frac{\pi}{2} - \mu\right) \\ \kappa_{max}^{-1} + R_\Omega \sin\left(-\frac{\pi}{2} - \mu\right) \\ 0 \\ 0 \end{pmatrix}. \qquad (6)$$

(ii) Considering that $q_2$ is the end configuration of the forward left CT, one can immediately determine the center $\Omega_2$ of the CC Circle $C_l^-(q_2)$.
(iii) For a certain $x^*$, the CC circle $C_r^+(q_s)$ has a center $\Omega_1(x^*)$, which is uniquely defined by $x^*$. On the other hand, the CC circle $C_r^+(q_s)$, corresponding to the first right CT starting from $q_s$, should be tangent to $C_l^-(q_2)$. Therefore, $x^*$ can be determined by solving the following nonlinear equation

$$\|\Omega_1 - \Omega_2\| = 2R_\Omega, \quad -M \leq x^* < 0, \qquad (7)$$

where $M$ is a constant.
(iv) With $x^*$, $\Omega_1 = (x_{\Omega_1}, y_{\Omega_1})$ and $\Omega_2 = (x_{\Omega_2}, y_{\Omega_2})$, we compute an auxiliary angle $\alpha$

$$\alpha = \arctan\left(\frac{y_{\Omega_2} - y_{\Omega_1}}{x_{\Omega_2} - x_{\Omega_1}}\right).$$

The deflection of the two CTs are given by $\delta$ and $-\delta$ accordingly, where $\delta = \alpha - \pi/2 + \mu$. The length of the straight line segment is given by $x^* - x_0$.

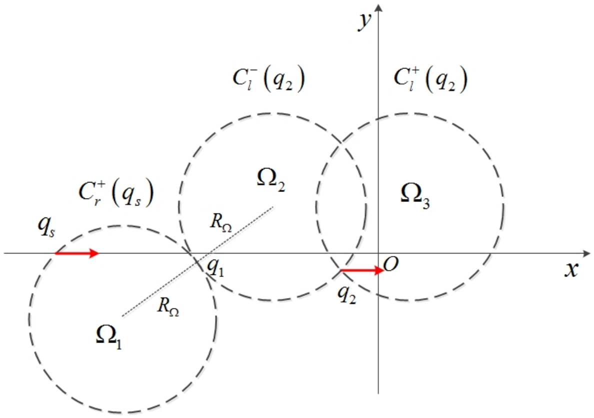

Fig. 4: $SC$ transition scheme

*2) SC Transition Algorithm:* Algorithm 1 summarizes the previous procedure. The $CCP - SC$ algorithm takes the initial and final configurations $q_0, q_f$, along with the error bound $\epsilon$, as inputs. The initial design parameter $\sigma_{\max}^0$ is selected in such a way that $\theta > 2\delta_c$ is satisfied. First, the $CCP - SC$ algorithm computes (lines 2 to 9) an appropriate $\sigma_{\max}$ such that $|y_2| \leq \epsilon$ to guarantee that $\mathcal{P}_{CC} \subseteq B(\mathcal{P}_{RS}, \epsilon)$. After obtaining $\sigma_{\max}$, the $CCP - SC$ algorithm computes (lines 10 to 14) the corresponding $x^*$. As explained in the computation procedure, $x^*$ should satisfy both (7) and the path constraint $x_0 < x^* < 0$. We reduce (7) to the equation in Line 13 based on simple geometric analysis. Once a proper $x^*$ is obtained, the iteration loop terminates and the $CCP - SC$ algorithm computes and outputs the CC path $\mathcal{P}_{CC}$ accordingly (lines 15 to 16); otherwise, Algorithm 1 increases the value of $\sigma_{\max}$ and updates the value of $x^*$.

### *B. CC Transition*

In the RS path classes, two circular arcs of radius $\kappa_{\max}^{-1}$ can be connected with or without a cusp. Here we treat a $CC$ connection (no cusp). Mathematical formulation of the $CC$ transition problem is stated as follows.

*Problem 3:* Let a simple RS path $\mathcal{P}_{RS}^{CC}$ consist of

(i) *A circular arc* $C_1$ which starts from the origin $q_0 = (0, 0, 0, 0)$ and ends at $A$. The radius and angle of $C_1$ are given by $\kappa_{\max}^{-1}$ and $\theta_1$, respectively.
(ii) *A circular arc* $C_2$ which is tangent to $C_1$ at $A$, moves in the same direction as $C_1$, and has the radius and angle given by $\kappa_{\max}^{-1}$ and $\theta_2$, respectively.

Construct a CC path $\mathcal{P}_{CC}$ which remains in $B(\mathcal{P}_{RS}^{CC}, \epsilon)$ while satisfying conditions (i)-(ii) in Problem 1.

**Algorithm 1** $CCP - SC$ Algorithm

```
Input: Error bound $\epsilon$, initial steering rate $\sigma^0_{\max}$, steering rate increment $\Delta\sigma$, iteration step $N$, initial configuration $q_0 = (x_0, 0, 0, 0)$ with $x_0 < 0$.
Output: A continuous curvature path $\mathcal{P}_{CC}$ connecting $q_0$ and $q_f$, steering rate $\sigma_{\max}$
1: Initialization: $k = 0$
2: repeat
3:     $\sigma^k_{\max} = \sigma^0_{\max} + k\Delta\sigma$
4:     Compute $R^k_\Omega$ and $\mu^k$ with respect to $\sigma^k_{\max}$ according to (5)
5:     Compute $q_2 = (x_2, y_2, 0, 0)$ according to (6)
6:     if $|y_2| > \epsilon$ then
7:         $k = k + 1$
8:     end if
9: until $|y_2| \le \epsilon$
10: repeat
11:     $\sigma^k_{\max} = \sigma^0_{max} + k\Delta\sigma$
12:     Compute the center $\Omega_2 = (x_{\Omega_2}, y_{\Omega_2})$ of $C^-_l(q_2)$
13:     Solve the equation
            $$\left(\frac{x_2 + x^*}{2} - x_{\Omega_1}\right)^2 + \left(\frac{y_2}{2} - y_{\Omega_1}\right)^2 = (R^k_\Omega)^2$$
14: until $x_0 < x^* < 0$ and $k \le N$
15: Compute $\mathcal{P}_{CC}$
16: return $\mathcal{P}_{CC}$ and $\sigma_{\max} = \sigma^k_{\max}$
```

For illustration purpose, we assume that $\theta_1 \in [0, \pi]$ (counterclockwise) and $\theta_2 \in [0, \pi]$ (clockwise). This scenario is represented by Fig. 5. Centers of $C_1$ and $C_2$ are given by

$$O_1 = \begin{pmatrix} 0 \\ \kappa^{-1}_{\max} \end{pmatrix}, \quad O_2 = \begin{pmatrix} 2\kappa^{-1}_{\max} \sin\theta_1 \\ \kappa^{-1}_{\max} - 2\kappa^{-1}_{\max} \cos\theta_1 \end{pmatrix}.$$

The final configuration of the arc $C_2$ is then obtained as

$$\begin{aligned} q_f = {} & (2\kappa^{-1}_{\max} \sin\theta_1 + \kappa^{-1}_{\max} \sin(\theta_2 - \theta_1), \\ & \kappa^{-1}_{\max} - 2\kappa^{-1}_{\max} \cos\theta_1 + \kappa^{-1}_{\max} \cos(\theta_2 - \theta_1), \theta_1 - \theta_2, 0). \end{aligned} \tag{8}$$

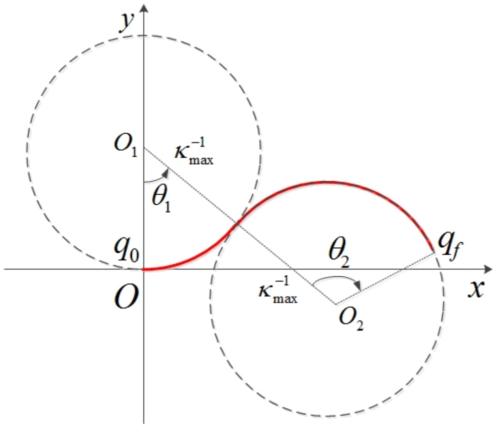

Fig. 5: A simple RS path: $CC$ type

*1) CC Transition Scheme:* Solving Problem 3 is similar to computing a CC path that connects configurations $q_0$ and $q_f$. We propose a CC path of the pattern $S|CC$ to solve Problem 3, where $S$ and $C$ denotes line segments and CT, respectively. Specifically, the proposed CC path is composed of:

(i) $S$: a backward line segment that starts from $q_0$ and ends at a configuration $q_s = (x^*, 0, 0, 0), -\epsilon \le x^* < 0$;
(ii) $CT_1$: a forward left CT with a deflection $\delta_1$ that starts from $q_s$ and ends at a configuration $q_1 = (x_1, y_1, \delta_1, 0)$;
(iii) $CT_2$: a forward right CT with a deflection $\delta_2 = \theta_1 - \theta_2 - \delta_1$ that starts from $q_1$ and ends at $q_f$.

Given an appropriate $\sigma_{\max}$, the following procedure can be employed to compute transition parameters $x^*$, $x_1$, $y_1$, $\delta_1$ and $\delta_2$. Please refer to Fig. 6 for further illustration.

(i) With $CT_2$ ending at $q_f$, given by (8), we have the center $\Omega_2 = (x_{\Omega_2}, y_{\Omega_2})$ of the CC Circle $C^-_r(q_f)$.
(ii) Since $CT_1$ starts from $q_s$, the center $\Omega_1(x^*)$ of CC Circle $C^+_l(q_s)$ is a vector-valued function of $x^*$.
(iii) CC Circles $C^+_l(q_s)$ and $C^-_r(q_f)$ must be tangent to each other. Towards this end, $x^*$ shall satisfy

$$\|\Omega_1(x^*) - \Omega_2\| = 2R_\Omega, \quad -\epsilon \le x^* < 0, \tag{9}$$

where $R_\Omega$ is given by (5).
(iv) Given $x^*$ solved from (9), $\Omega_1 = (x_{\Omega_1}, y_{\Omega_1})$ can be determined. Compute the auxiliary angle $\alpha$ as follows

$$\alpha = \arctan\left(\frac{y_{\Omega_2} - y_{\Omega_1}}{x_{\Omega_2} - x_{\Omega_1}}\right).$$

The deflections of $CT_1$ and $CT_2$ are given by $\delta_1 = \alpha + \pi/2 - \mu$, and $\delta_2 = \theta_1 - \theta_2 - \delta_1$, respectively, while the length of the line segment is obtained as $|x^*|$.

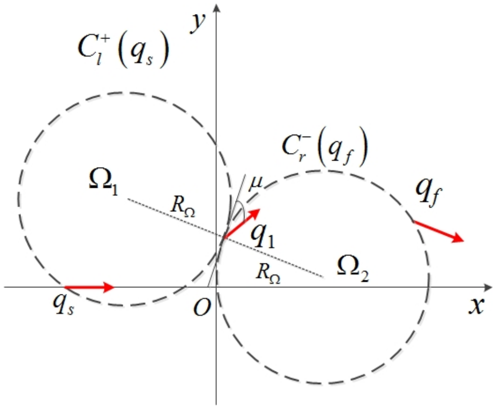

Fig. 6: $CC$ transition scheme

*2) CC Transition Algorithm:* We summarize the computation procedure of the $S|CC$ path that connects $q_0$ and $q_f$ as the $CCP - CC$ algorithm, as shown in Algorithm 2. Intuitively, the $CCP - CC$ algorithm computes an appropriate $x^*$ in an iterative manner such that (9) can be satisfied. For such a purpose, at the $k$-th iteration step, the $CCP - CC$ computes $R_\Omega$ and $\mu$ with respect to $\sigma^k_{\max} = \sigma^0_{\max} + k\Delta\sigma$ (Lines 3 to 4). Next, the center $\Omega_2$ of $C^-_r(q_f)$ is obtained (Line 5). On the other hand, from a simple geometric reasoning, the center $\Omega_1$ of $C^+_l(q_s)$ can be obtained from $x^*$ and $\Omega_0$ of

$C_l^+(q_0)$ (Lines 6-7). Based on the coordinates of $\Omega_1$, (9) can then be reduced to the equation presented in Line 8 of the $CCP-CC$ algorithm. Solving this equation yields a valuation of $x^*$; and $x^*$ can be accepted whenever $|x^*| < \epsilon$ (Lines 9-12). Afterwards, the desired $\mathcal{P}_{CC}$ can be computed in terms of $x^*$ and $\sigma_{\max}^k$ accordingly.

**Algorithm 2** $CCP-CC$ Algorithm

```
Input: Error bound $\epsilon$, initial steering rate $\sigma_{\max}^0$, steering
    rate increment $\Delta\sigma$, iteration step $N$, configurations $q_0$
    and $q_f$.
Output: A continuous curvature $S|CC$ path $\mathcal{P}_{CC}$ connecting $q_0$ and $q_f$, steering rate $\sigma_{\max}$
 1: Initialization: $k = 0$
 2: repeat
 3:     $\sigma_{\max}^k = \sigma_{\max}^0 + k\Delta\sigma$
 4:     Compute $R_\Omega^k$ and $\mu^k$ w.r.t. $\sigma_{\max}^k$ according to (5)
 5:     Compute the center $\Omega_2^k = (x_{\Omega_2}^k, y_{\Omega_2}^k)$ of $C_r^-(q_f)$ with
        $R_\Omega^k$ and $\mu^k$
 6:     Compute the center $\Omega_0^k = (x_{\Omega_0}^k, y_{\Omega_0}^k)$ of $C_l^+(q_0)$ with
        $R_\Omega^k$ and $\mu^k$
 7:     Let $\Omega_1^k = (x_{\Omega_0}^k + x^*, y_{\Omega_0}^k)$ be the center of $C_l^+(q_1)$
 8:     Determine $x^*$ by solving
            $(x_{\Omega_0}^k + x^* - x_{\Omega_2}^k)^2 + (y_{\Omega_0}^k - y_{\Omega_2}^k)^2 = (2R_\Omega^k)^2$
 9:     if $|x^*| > \epsilon$ or $x^* > 0$ then
10:         $k = k + 1$
11:     end if
12: until $|x^*| \le \epsilon$ and $k \le N$
13: Compute $\mathcal{P}_{CC}$ from $\sigma_{\max}^k$ and $x^*$
14: return $\mathcal{P}_{CC}$ and $\sigma_{\max} = \sigma_{\max}^k$
```

### C. $C|C$ Transition

When a cusp emerges in an RS path, we design a corresponding CC path by constructing $C|C$ transition. The $C|C$ transition problem is stated as follows.

*Problem 4:* Let a simple RS path $\mathcal{P}_{RS}^{C|C}$ consist of

(i) *A circular arc* $C_1$ *that starts from the origin* $q_0 = (0,0,0,0)$ *with the radius and angle of* $C_1$ *given by* $\kappa_{max}^{-1}$ *and* $\theta_1$*, respectively.*

(ii) *A circular arc* $C_2$ *that is tangent to* $C_1$ *at point* $A$*, and moves in the opposite direction as in* $C_1$*. The radius and angle of* $C_2$ *are given by* $\kappa_{max}^{-1}$ *and* $\theta_2$*, respectively.*

Construct a CC path $\mathcal{P}_{CC} \subseteq B(\mathcal{P}_{RS}^{C|C}, \epsilon)$ while satisfying conditions (i)-(ii) in Problem 1.

For illustration purpose, we assume that $\theta_1 \in [0, \pi]$ (counterclockwise) and $\theta_2 \in [0, \pi]$ (counterclockwise). This scenario is shown in Fig. 7.

Centers of circular arcs $C_1$ and $C_2$ are computed similarly as in the $CC$ transition case. The path $\mathcal{P}_{RS}^{C|C}$ ends at the configuration

$$\begin{aligned} q_f &= (2\kappa_{\max}^{-1}\sin\theta_1 - \kappa_{\max}^{-1}\sin(\theta_1+\theta_2) \\ &\kappa_{\max}^{-1} - 2\kappa_{\max}^{-1}\cos\theta_1 + \kappa_{\max}^{-1}\cos(\theta_1+\theta_2), \theta_1+\theta_2, 0). \end{aligned} \tag{10}$$

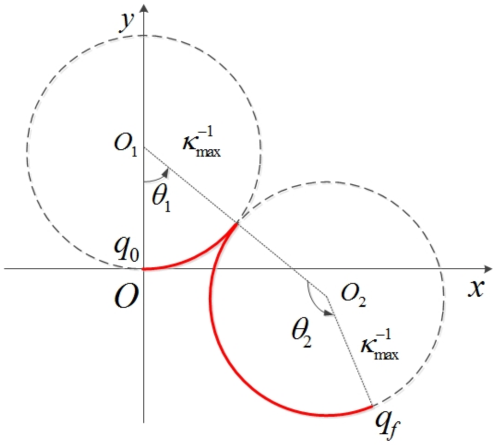

Fig. 7: A simple RS path: $C|C$ type

*1) $C|C$ Transition Scheme:* We propose to construct a CC path of the pattern $S|C|C$ that connects $q_0$ to $q_f$. In particular, the proposed CC path consists of

(i) $S$: a backward line segment from $q_0$ to a configuration $q_s = (x^*, 0, 0, 0)$, $-\epsilon \le x^* < 0$;

(ii) $CT_1$: a forward left CT with a deflection $\delta_1$ that starts from $q_s$ and ends at a configuration $q_1 = (x_1, y_1, \delta_1, 0)$;

(iii) $CT_2$: a backward right CT with a deflection $\delta_2 = \theta_1 + \theta_2 - \delta_1$ that starts from $q_1$ and ends at $q_f$.

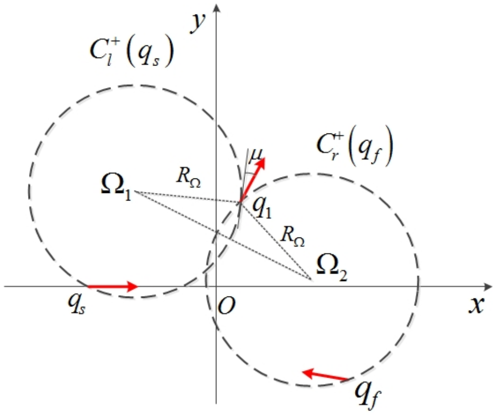

Fig. 8: $C|C$ transition scheme

Given $\sigma_{\max}$, the following procedure can be employed to determine transition parameters $x^*$, $x_1$, $y_1$, $\delta_1$ and $\delta_2$. Please refer to Fig. 8 for illustration.

(i) With $CT_2$ ending at $q_f$, given by (10), we have coordinates of the center of $C_r^+(q_f)$ as $\Omega_2 = (x_{\Omega_2}, y_{\Omega_2})$.

(ii) With $CT_1$ starting at $q_s$, the center $\Omega_1(x^*)$ of CC circle $C_l^+(q_s)$ is given by a vector-valued function of $x^*$.

(iii) Based on $\mu-$tangency conditions, CC Circles $C_l^+(q_s)$ and $C_r^+(q_f)$ must be $\mu-$intersecting. That is, $x^*$ shall ensure

$$\|\Omega_1(x^*) - \Omega_2\| = 2R_\Omega\cos\mu, \quad -\epsilon \le x^* < 0. \tag{11}$$

(iv) Given $x^*$ solved from (11), $\Omega_1 = (x_{\Omega_1}, y_{\Omega_1})$ can be determined. Compute the auxiliary angle $\alpha$ as follows:

$$\alpha = \arctan\left(\frac{y_{\Omega_2} - y_{\Omega_1}}{x_{\Omega_2} - x_{\Omega_1}}\right).$$

The deflections of $CT_1$ and $CT_2$ are given by $\delta_1 = \alpha + \pi/2$, and $\delta_2 = \theta_1 + \theta_2 - \delta_1$, respectively; whereas the length of the line segment is given by $|x^*|$.

*2) $C|C$ Transition Algorithm:* We summarize the aforementioned computation procedure of the $S|C|C$ as the $CCP - C|C$ algorithm, as shown in Algorithm 3. Intuitively, the $CCP - C|C$ algorithm determines $x^*$ iteratively such that it solves (11). Towards this end, the $CCP - C|C$ first computes $R_\Omega^k$ and $\mu^k$ with respect to $\sigma_{\max}^k = \sigma_{\max}^0 + k\Delta\sigma$ at the $k$-th iteration step (Lines 3 to 4). Next, the center $\Omega_2$ of $C_r^+(q_f)$ is obtained (Line 5). In addition, the center $\Omega_1$ of $C_l^+(q_s)$ can be computed based on the center $\Omega_0$ of $C_l^+(q_0)$ (Lines 6-7). From the coordinates of $\Omega_1$, (11) can then be reduced to the equation presented in Line 8. Solving this equation yields $x^*$, which can be accepted whenever $|x^*| < \epsilon$ is satisfied before the iteration terminates (Lines 9-12). Afterwards, the desired $\mathcal{P}_{CC}$ can be computed in terms of $x^*$ and $\sigma_{\max}^k$ accordingly.

**Algorithm 3** $CCP - C|C$ Algorithm

```
Input: Error bound $\epsilon$, initial steering rate $\sigma_{\max}^0$, steering
    rate increment $\Delta\sigma$, iteration step $N$, configurationss $q_0$
    and $q_f$.
Output: A continuous curvature $S|C|C$ path $\mathcal{P}_{CC}$ connect-
    ing $q_0$ and $q_f$, steering rate $\sigma_{\max}$
 1: Initialization: $k = 0$
 2: repeat
 3:   $\sigma_{\max}^k = \sigma_{\max}^0 + k\Delta\sigma$
 4:   Compute $R_\Omega^k$ and $\mu^k$ with $\sigma_{\max}^k$ according to (5)
 5:   Compute the center $\Omega_2^k = (x_{\Omega_2}^k, y_{\Omega_2}^k)$ of $C_r^+(q_f)$ with
      $R_\Omega^k$ and $\mu^k$
 6:   Compute the center $\Omega_0^k = (x_{\Omega_0}^k, y_{\Omega_0}^k)$ of $C_l^+(q_0)$ with
      $R_\Omega^k$ and $\mu^k$
 7:   Let $\Omega_1^k = (x_{\Omega_0}^k + x^*, y_{\Omega_0}^k)$ be the center of $C_l^+(q_1)$
 8:   Determine $x^*$ by solving
      $(x_{\Omega_0}^k + x^* - x_{\Omega_2}^k)^2 + (y_{\Omega_0}^k - y_{\Omega_2}^k)^2 = (2R_\Omega^k \cos\mu^k)^2$
 9:   if $|x^*| > \epsilon$ or $x^* > 0$ then
10:     $k = k + 1$
11:   end if
12: until $|x^*| \le \epsilon$ and $k \le N$
13: Compute $\mathcal{P}_{CC}$ from $\sigma_{\max}^k, x^*$
14: return $\mathcal{P}_{CC}$ and $\sigma_{\max} = \sigma_{\max}^k$
```

## IV. Simulation Results

In this section, simulation is conducted to verify the effectiveness of the aforementioned computation schemes and algorithms, where three types of transition are considered.

For the $SC$ transition case, we assume that $\kappa_{\max} = 1$, $\sigma_{\max} = 1$ and $\theta = \pi/3$. The line and the circular arc are shown in Fig. 9. Based on the proposed computation procedure, we have $x^* = -2.5616$, and the centers of CC Circles $C_l^+(q_2)$, $C_l^-(q_2)$ and $C_r^+(q_s)$, shown in Fig. 9, are obtained as $\Omega_1 = (-2.0657, -1.0413), \Omega_2 = (-0.9917, 1), \Omega_3 = (0, 1)$. The auxiliary angle is $\alpha = 1.0864rad$ and the deflection of the right CT is $\delta = -0.04rad$. The planned CC path is zoomed in Fig. 10.

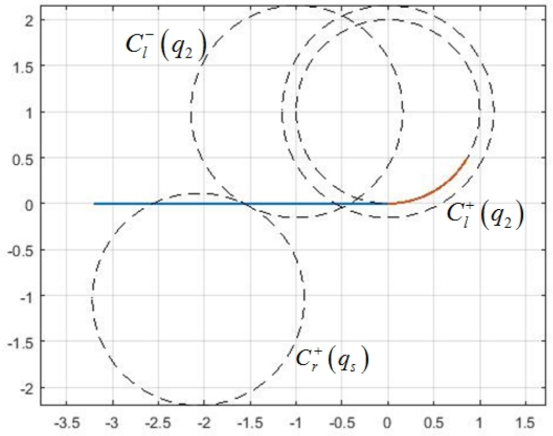

Fig. 9: RS path, CC circles and CC path: $SC$ case

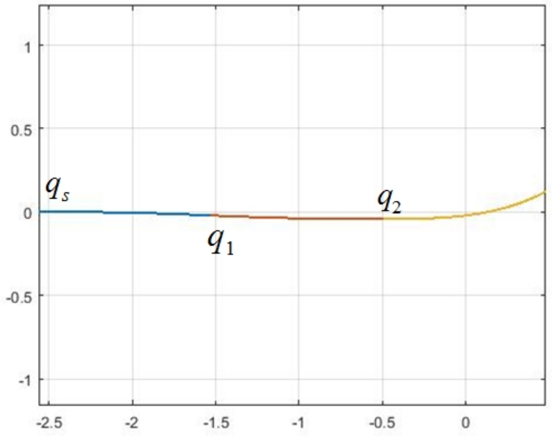

Fig. 10: CC path: $SC$ case

For the $CC$ transition case, we assume that $\kappa_{\max} = 1$ and $\sigma_{\max} = 5$. The angular value of the counterclockwise circular arc is $\theta_1 = \pi/3$ and the angular value of the clockwise circular arc is $\theta_2 = \pi/2$. The two connecting circular arcs are shown in Fig. 11. We first calculate the center of the CC Circle $C_r^-(q_f)$ and have $\Omega_2 = (1.6446, 0.0485)$. Next, we solve (9) and have $x^* = -0.2286$. Thus, the center of the CC Circle $C_l^+(q_s)$ is obtained as $\Omega_1 = (-0.1286, 1.0017)$. The CC Circles are shown in Fig. 11 (in blue dashed lines). The auxiliary angle and deflections of two CTs are obtained: $\alpha = -0.4932rad, \delta_1 = 0.9781rad, \delta_2 = -1.5017rad$. The $S|CC$ path are represented by yellow solid lines in Fig. 11.

Regarding the $C|C$ transition case, we take that $\kappa_{\max} = 1$,

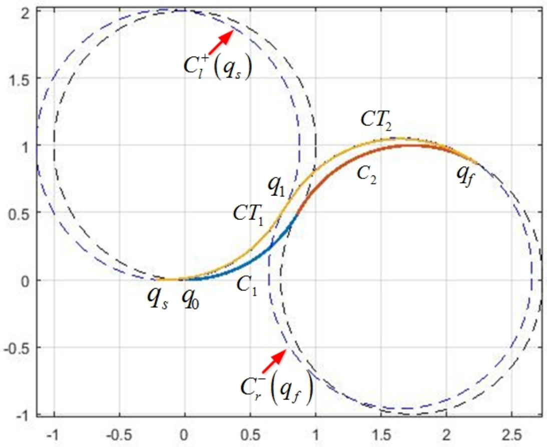

Fig. 11: RS path, CC circles and CC path: $CC$ case

$\sigma_{\max} = 5$, $\theta_1 = \pi/3$, and $\theta_2 = \pi/2$. The $C|C$ RS path is shown in Fig. 12. We first compute the center of the CC Circle $C_r^+(q_f)$ and have $\Omega_2 = (1.6463, 0.0514)$. Next, we solve (11) for $x^*$ and have $x^* = -0.2172$. The auxiliary angle and deflections of two CTs are computed: $\alpha = -0.4942rad, \delta_1 = 1.0766rad, \delta_2 = 1.5414rad$. The center of the CC Circle $C_l^+(q_s)$ is obtained as $\Omega_1 = (-0.1172, 1.0017)$. Blue dashed circles in Fig. 12 show the CC Circles, while the planned $S|C|C$ path is represented by yellow solid lines.

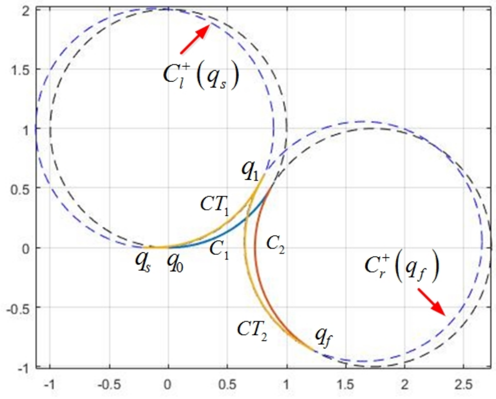

Fig. 12: RS path, CC circles and CC path: $C|C$ case

## V. Conclusion

This paper proposed a real-time continuous curvature path planning method for car-like robots. The proposed method results in almost equivalent computational efficiency and reliability as Reeds-Shepp's based path planning by post-processing Reeds-Shepp's paths. The post-processing stage, different from conventional optimization approaches, resorts to geometric $\mu-$tangency conditions, which not only allow a majority of planning work done offline, but also enable development of convergence guaranteed algorithms. Effectiveness of the proposed path planning method was validated by simulation.

## References

[1] M. D. Berkemeier, "System and method for controlling a vehicle," US2016/03133735A1, 2016.

[2] T. Fraichard and A. Scheuer, "From Reeds and Shepp's to continuous-curvature paths," *IEEE Trans. Robot.*, vol. 20, no. 6, pp. 1025–1035, Dec. 2004.

[3] H. M. Choset, K. M. Lynch, S. Hutchinson, G. A. Kantor, W. Burgard, L. E. Kavraki, and S. Thrun, *Principles of Robot Motion: Theory, Algorithms, and Implementation*. Cambridge, MA: MIT Press, 2005.

[4] S. M. LaValle, *Planning algorithms*. Cambridge, UK: Cambridge University Press, 2006.

[5] G. E. Fainekos, A. Girard, H. Kress-Gazit, and G. J. Pappas, "Temporal logic motion planning for dynamic robots," *Automatica*, vol. 45, no. 2, pp. 343–352, 2009.

[6] P. R. Giordano, M. Vendittelli, J.-P. Laumond, and P. Souéres, "Nonholonomic distance to polygonal obstacles for a car-like robot of polygonal shape," *IEEE Trans. Robot.*, vol. 22, no. 5, pp. 1040–1047, 2006.

[7] L. E. Dubins, "On curves of minimal length with a constraint on average curvature, and with prescribed initial and terminal positions and tangents," *American Journal of Mathematics*, pp. 497–516, 1957.

[8] J. A. Reeds and L. A. Shepp, "Optimal paths for a car that goes both forwards and backwards," *Pacific Journal of Mathematics*, vol. 145, no. 2, pp. 367–393, 1990.

[9] J.-P. Laumond, P. E. Jacobs, M. Taïx, and R. M. Murray, "A motion planner for nonholonomic mobile robots," *IEEE Trans. Robot. Automat.*, vol. 10, no. 5, pp. 577–593, Oct. 1994.

[10] H. Vorobieva, S. Glaser, N. Minoiu-Enache, and S. Mammar, "Automatic parallel parking in tiny spots: path planning and control," *IEEE Trans. Intell. Transp. Syst.*, vol. 16, no. 1, pp. 396–410, 2015.

[11] J. D. Boissonnat, A. Cerezo, and J. Leblond, "A note on shortest paths in the plane subject to a constraint on the derivative of the curvature," INRIA, France, Tech. Rep. RR-2160, 1994.

[12] H. J. Sussmann, "The markov-dubins problem with angular acceleration control," in *Proc. 1997 ICRA*, May. 1997, pp. 2636–2643.

[13] A. Scheuer and C. Laugier, "Planning sub-optimal and continuous-curvature paths for car-like robots," in *Proc. 1998 IROS*, 1998, pp. 25–31.

[14] J. Dai and Y. Wang, "Existence conditions of a class of continuous curvature paths," in *the 36th Chinese Control Conf.*, Jul. 2017, p. under review.

[15] K. Yang and S. Sukkarieh, "An analytical continuous-curvature path-smoothing algorithm," *IEEE Trans. Robot.*, vol. 26, no. 3, pp. 561–568, 2010.

[16] E. Bakolas and P. Tsiotras, "On the generation of nearly optimal, planar paths of bounded curvature and bounded curvature gradient," in *Proc. 2009 ACC*, Jun. 2009, pp. 385–390.

[17] L. Kavraki, P. Svestka, J.-C. Latombe, and M. Overmars, "Probabilistic roadmaps for path planning in high-dimensional configuration spaces," *IEEE Trans. Robot. Automat.*, vol. 12, no. 4, pp. 566–580, Aug 1996.